Int. J. Therm. Sci. (2001) 40, 804–815

S1290-0729(01)01267-4/FLA

Low-Reynolds number supersonic diffuser for a plasma-heated wind tunnel

Rodolfo Monti, Diego Paterna, Raffaele Savino *, Antonio Esposito

Department of Space Science and Engineering (DISIS), University of Naples "Federico II", P.le Tecchio 80, Naples, Italy

(Received 6 July 2000, accepted 10 November 2000)

Abstract — The diffuser is one of the main components of a hypersonic wind tunnel, having the task to achieve the maximum pressure recovery. This is accomplished with an *efficiency* that characterises the performances of the diffuser, and that is Reynolds number dependent.

The behaviour of supersonic diffusers at low Reynolds numbers has not been extensively investigated in literature, but it is very important, since it may affect the performance of the entire wind tunnel.

The experimental results presented in this paper have been obtained with a 40 kW plasma wind tunnel available at the Department of Space Science and Engineering (DISIS) at the University of Naples.

The *Fluent* code has been used to numerically simulate the flow inside each component of the facility. Computations have been carried out for different values of the downstream pressure of the diffuser (for fixed values of total enthalpy and mass flow rate).

The numerical and experimental results are in good agreement. © 2001 Éditions scientifiques et médicales Elsevier SAS

diffuser / plasma wind tunnel / arcjet / supersonic flow / Navier–Stokes equations / finite volume technique

Nomenclature

H	specific total enthalpy at the nozzle inlet (torch exit)	$\mathrm{MJ\cdot kg^{-1}}$
h	specific enthalpy	$\mathrm{MJ\cdot kg^{-1}}$
$\dot{m}$	mass flow rate	$\mathrm{g\cdot s^{-1}}$
c_p	specific heat at constant pressure	$\mathrm{J\cdot kg^{-1}\cdot K^{-1}}$
c_v	specific heat at constant volume	$\mathrm{J\cdot kg^{-1}\cdot K^{-1}}$
VI	power provided by the torch	kW
ΔT	temperature increase	K
Re	Reynolds number	
M	frozen Mach number	
T	thermodynamic temperature	K
m	mass fraction	
M	molecular weight	$\mathrm{kg\cdot kmole^{-1}}$
p	pressure	Pa
R_0	universal gas constant	$\mathrm{J\cdot kmole^{-1}\cdot K^{-1}}$
R	mixture constant	$\mathrm{J\cdot kg^{-1}\cdot K^{-1}}$
D	diffusion coefficient	$\mathrm{m^2\cdot s^{-1}}$
K	reaction rate constant ($\mathrm{m^3\cdot kmole^{-1}\cdot s^{-1}}$ for the forward reaction rate, $\mathrm{m^6\cdot kmole^{-2}\cdot s^{-1}}$ for the backward reaction rate)	
k	turbulence kinetic energy	$\mathrm{J\cdot kg^{-1}}$
I	turbulence intensity	$\mathrm{m\cdot s^{-1}}$
l	turbulence length scale	m
u, v, V	axial, radial velocity components, velocity magnitude	$\mathrm{m\cdot s^{-1}}$
T	wall temperature	K
A	nozzle inlet area	$\mathrm{m^2}$
y	normal co-ordinate to the wall	m
r	radial co-ordinate	m
x	axial co-ordinate	m
$\mathrm{N_2}$, N, $\mathrm{N^+}$	Nitrogen, atomic Nitrogen and ionised atomic Nitrogen	

Greek symbols

γ	ratio of the mixture specific heats $= c_\mathrm{p}/c_\mathrm{v}$	
ρ	density	$\mathrm{kg\cdot m^{-3}}$
λ	thermal conductivity	$\mathrm{W\cdot m^{-1}\cdot K^{-1}}$
μ	molecular viscosity	$\mathrm{kg\cdot m^{-1}\cdot s^{-1}}$
γ	efficiency of the third body	

* Correspondence and reprints.
E-mail addresses: monti@unina.it (R. Monti), paterna@unina.it (D. Paterna), rasavino@unina.it (R. Savino).

υ	stoichiometric coefficient	
ε	turbulence dissipation rate	$\mathrm{J{\cdot}Kg^{-1}{\cdot}s^{-1}}$

Subscripts

0	stagnation conditions at the nozzle inlet
ch	chemical contribution
N	atomic Nitrogen
N_2	Nitrogen
H_2O	water
T	translational contribution
V	vibrational contribution
D	diffuser throat diameter
D_N	nozzle inlet diameter
cr	critical conditions
ref	reference conditions (288.15 (K))
i	species *i*
w	wall conditions

Superscripts

(i)	initial or torch inlet conditions

1. INTRODUCTION

One of the main components of a hypersonic wind tunnel is the diffuser. The diffuser has the task of converting the kinetic energy of the flow into thermal energy with a minimum loss (i.e., to achieve the maximum pressure recovery). A good efficiency of the diffuser results in a reduced overall power requirement when running the wind tunnel.

The Reynolds number plays an important role in the behaviour of a supersonic diffuser, especially between values of 10^3 and $3{\cdot}10^5$; in this range it is very difficult to predict the performance of the diffuser.

CIRA (Italian Centre for Aerospace Research), which is assembling the SCIROCCO, a 70 MW plasma wind tunnel, expects a dramatic reduction of the efficiency for Reynolds numbers below $5{\cdot}10^4$. During the design phase of SCIROCCO, Fluidyne carried out an experimental test campaign on the SCIROCCO diffuser [1, 2], at low Reynolds numbers; the results have been obtained in a 1 : 6 scaled down version of the SCIROCCO diffuser. During the tests, the minimum Reynolds number (at the nozzle exit) was $4{\cdot}10^4$, lower values are foreseen for SCIROCCO operating at smaller mass flow rates.

The experimental data that correlate the numerical simulations have been obtained with the plasma wind tunnel HEBDAF (High Enthalpy Blow Down Arc Facility), which operates at DISIS and runs at very low Reynolds numbers ($1000 < Re_D < 6000$). The diffuser mounted in HEBDAF reproduces the SCIROCCO diffuser at a scale of 1 : 60.

The Fluent code, distributed by Fluent Inc., has been used for the numerical calculations.

The lack of experimental data concerning the chemical composition of the gas at the inlet of the HEBDAF nozzle has forced the authors to make a number of assumptions regarding the thermo-chemical conditions of the gas at the torch exit. In particular, the initial assumption of chemical equilibrium and uniformity of the flow that enters the nozzle leads to a poor comparison with the experimental results. Therefore, we have simulated the thermo-fluid-dynamic field inside the plasma torch, assuming a very simplified model of the electric arc. This analysis, supported by a bibliographic investigation of the electric arc heaters, allowed us to obtain the missing parameters needed for the numerical simulations of the diffuser.

This work is divided into three parts:

In the first part we describe the experimental facility and the measurements performed at different test conditions.

In the second part we present the mathematical/physical model that describes the flow, in particular the thermodynamics, thermo-chemical and turbulence models. We further describe the techniques employed by the Fluent code for the numerical solution of the Navier–Stokes equations.

In the third part we describe the numerical results, and we compare the experimental pressures along the diffuser wall with the values obtained via the numerical computations.

2. THE EXPERIMENTAL APPARATUS

The *High Enthalpy Blown Down Arc Facility* [3], (*figure 1*), is a continuous, open circuit, hypersonic wind tunnel, utilising an *"Arc-Jet"*.

The test gas is Nitrogen.

The gas from the high pressure cylinders flows between the electric arc electrodes. Successively, the plasma flows through a convergent-divergent nozzle ($A_u/A^* = 4$, $M_{exit} = 3$) where it expands until it reaches the test-chamber; the flow then goes through the diffuser and the heat exchanger, and finally it enters the system of vacuum pumps, that eject it into the surrounding environment.

In order to determine the mean value of the specific total enthalpy of the gas at the nozzle entrance, a balance

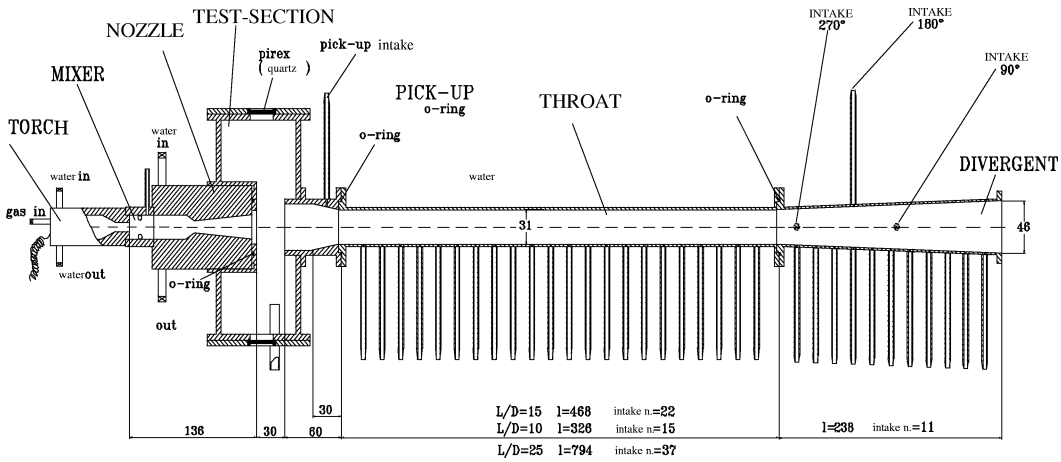

Figure 1. High Enthalpy Blow-Down Arc Facility (HEBDAF).

is made between the energy provided to the gas by the arc and the energy eliminated by the cooling water.

The specific total enthalpy of the flow at the nozzle inlet (torch exit) can therefore be expressed as follows:

$$H_0 = \frac{VI + c_{pN_2}\dot{m}_{N_2}T_{N_2}^{(i)} - c_{pH_2O}\dot{m}_{H_2O}\Delta T_{H_2O}}{\dot{m}_{N_2}} \qquad (1)$$

3. EXPERIMENTAL TESTS

Each experimental run includes an initial starting phase characterised by given values of the gas mass flow rate and of the electric arc power, and by a low-pressure value imposed at the diffuser exit by the system of vacuum pumps. The diffuser exit pressure is therefore gradually increased, and a shock wave system inside the diffuser is created, generating a subsonic flow. Increasing the exit pressure, the shock waves move upstream towards the diffuser inlet and the test-chamber.

The parameters that characterise the experimental tests are:

(a) The gas mass flow rate ($\dot{m}_{N_2}$, in the range 1–5 g·s^{-1});
(b) The power added to the gas by the electric arc (VI, between 5 and 40 kW);
(c) The specific total enthalpy at the nozzle inlet ($5 < H_0 < 25$ MJ·kg^{-1});
(d) The total pressure at the nozzle inlet ($13000 < p_0 < 130000$ Pa).

The corresponding values of the other relevant parameters in the flow field (plasma torch, nozzle, test chamber and diffuser) are:

(a) $1000 < Re_D < 10000$;
(b) $0 < M < 5$;
(c) $300 < T < 10000$ K.

Re_D is taken as an average of the values at the diffuser inlet and it is as follows:

$$Re_D = \frac{\rho V D}{\mu} = \frac{\dot{m}}{\mu}\frac{4}{\pi D} \qquad (2)$$

where μ is the mean value of the mixture viscosity at the diffuser inlet.

The frozen Mach number M is defined as:

$$M = V/a \qquad (3)$$

where a is the frozen speed of sound for the mixture:

$$a = \sqrt{\gamma RT} \qquad (4)$$

4. THE SIMULATION MODEL

For the numerical simulations a suitable thermophysical model has been introduced in the Fluent code [4], solving the Navier–Stokes equations via a finite-volume technique.

4.1. Thermodynamic model

Due to the high enthalpy values, the gas is partly dissociated; therefore it is treated as a binary mixture formed by molecular Nitrogen and atomic Nitrogen (N_2, N).

The component gases are assumed to be perfect gases, satisfying Dalton's Law:

$$\rho = \frac{p}{R_0 T \sum_i \frac{m_i}{M_i}} \tag{5}$$

where $R_0 = 8314$ J·kmole^{-1}·K^{-1}.

The temperatures that characterise the translational, rotational and vibrational degrees of freedom have all been assumed to be in equilibrium at the thermodynamic temperature T (i.e., the translational temperature).

The specific heats of the molecular and atomic Nitrogen, $c_{\mathrm{p,N}}(T)$, $c_{\mathrm{p,N_2}}(T)$, have been expressed as polynomial functions of the temperature:

$$c_{\mathrm{P_{N,N_2}}} = a_0 + \sum_{j=1}^{n} a_j T^j \tag{6}$$

The coefficients a_j, for $300 < T < 35000$ K, are reported in [5].

The specific enthalpy for the gas mixture is:

$$h = \sum_i m_i h_i = \sum_i m_i \left(h^0_{\mathrm{f},i} + \int_{T_{\mathrm{ref}}}^{T} c_{\mathrm{p},i}\, \mathrm{d}T \right) \tag{7}$$

where: $h^0_{\mathrm{f},i}$ is the formation enthalpy for the generic species i at the reference temperature ($h^0_{\mathrm{f,N_2}} = 0$, $h^0_{\mathrm{f,N}} =$ 4.7096E+08 J·kmole^{-1}).

4.2. Transport properties

The viscosity and the thermal conductivity of the species composing the mixture, expressed as polynomial functions of the temperature, are reported in [5].

The values of the viscosity and of the thermal conductivity for the mixture are obtained using the semi-empirical Wilke's rule in terms of the properties $\mu_i = \mu_i(T)$, $\lambda_i = \lambda_i(T)$, of the single species.

The mass diffusivity coefficient of each chemical species in the mixture is calculated using the kinetic theory of gases [6].

4.3. Chemical model

The reactions considered are the recombination and dissociation of Nitrogen:

$$\mathrm{N_2} + \mathrm{N_2} \quad \Longleftrightarrow \quad 2\mathrm{N} + \mathrm{N_2} \tag{8}$$

For the generic reaction the rate, constant K assumes Arrhenius' form:

$$K_j = A_j T^{\beta_j} \exp\left(-\frac{E_j}{R_0 T} \right) \tag{9}$$

where: A_j, B_j, E_j are constants; in this work we use the values of the Dunn–Kang model [6], which provides the values of both the forward and backward reaction rate constants.

4.4. Flow equations

The governing equations are the Navier–Stokes equations for axi-symmetric, compressible, reacting, turbulent flow. They include the balance equations for mass, species, x-momentum, r-momentum, and energy.

The standard k–ε model has been used as a turbulence model [4, 7, 8].

4.5. Boundary conditions

The mathematical problem is well posed once the boundary conditions have been completely assigned.

The physical domain has the form of a cylindrical duct (with variable section) and boundary conditions have to be assigned on the walls and on the inlet and outlet sections. A scheme of the computational domain is illustrated in *figure 2*. The origin of the axial co-ordinate x is located at the nozzle inlet.

Wall conditions:

(a) $u = 0$, $v = 0$;
(b) $T_{\mathrm{W}} = 400$ K;
(c) $(\frac{\partial m_i}{\partial y})_{y=0} = 0$ (non-catalytic condition); in fact, we have seen that the interior walls of the nozzle and the diffuser, which are made of copper, have, after performing several experimental tests, oxidised so we expect a poor catalytic behaviour of the walls.

Inlet conditions:

(a) Mass flow rate:

$$\dot{m} = \int \rho V \, \mathrm{d}A;$$

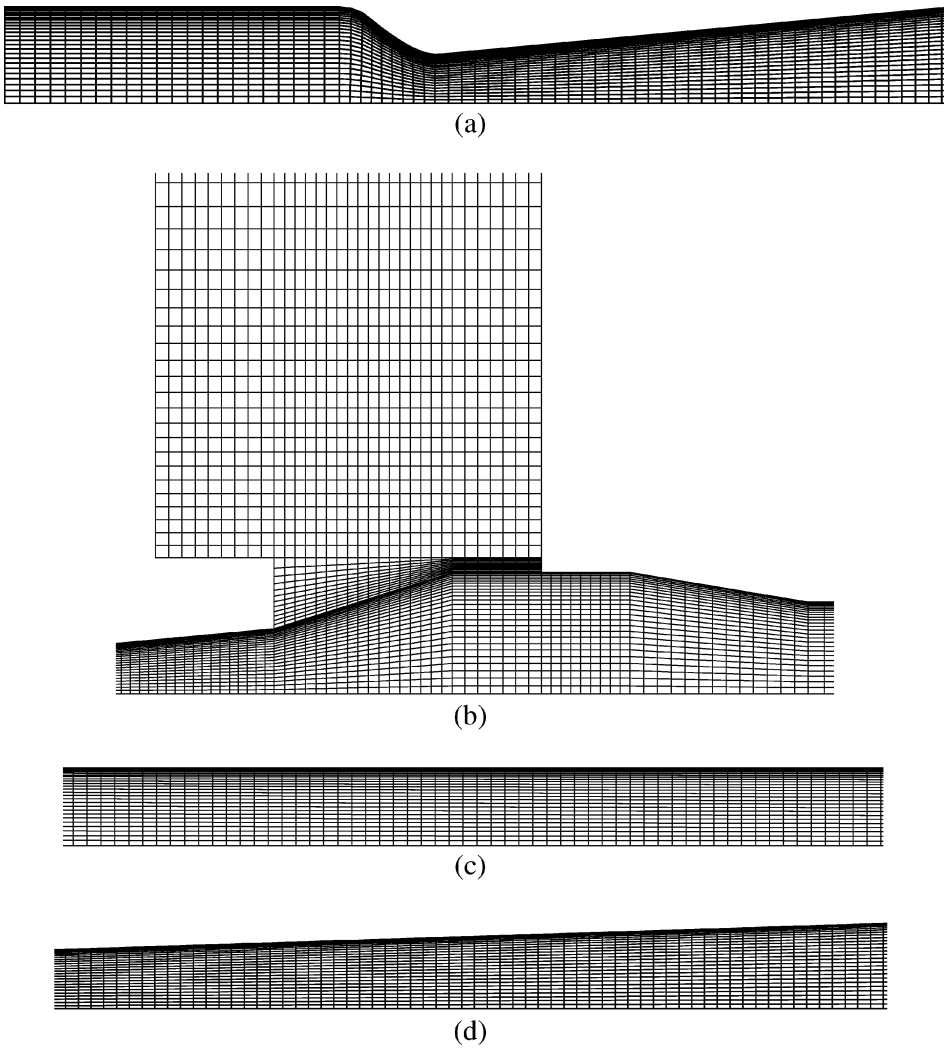

Figure 2. Mesh of the computational domain: (a) Nozzle; (b) Test chamber and diffuser pick-up; (c) diffuser throat; (d) diffuser divergent.

(b) Specific total enthalpy, H_0;

(c) Atomic Nitrogen mass fractions, m_{N};

(d) Pressure. We assume that the Mach number is 1 at the torch exit section; the pressure is thus assigned in such a way as to satisfy this condition. Indeed one may write:

$$\dot{m} = \rho V A = \frac{\gamma p}{\gamma RT} V A = \frac{\gamma p \cdot M \cdot A}{\sqrt{\gamma RT}} = \frac{\gamma p \cdot M \cdot A}{\sqrt{\gamma RT_0 (1 + ((\gamma - 1)/2) M^2)^{-1}}},$$

so that, for $M = 1$: $p = \frac{\dot{m}}{A}\sqrt{\frac{2RT_0}{\gamma(\gamma+1)}}$, where T_0 is related to the total enthalpy:

$$\int_{T_{\mathrm{ref}}}^{T_0} c_{\mathrm{p}}\, \mathrm{d}T = H_0$$

(e) The initial values for turbulent kinetic energy k and turbulence dissipation energy, ε, are obtained through empirical relations [8]. The turbulence intensity at the core of a fully-developed duct flow can be estimated from the following formula derived from an empirical

correlation for pipe flows:

$$I = 0.16 \cdot (Re_{D_N})^{-1/8} \tag{10}$$

In fully developed duct flows, l is restricted by the size of the duct, since the turbulent eddies cannot be larger than the duct. An approximate relationship between 1 and the physical size of the duct is:

$$l = 0.07 \cdot D_N \tag{11}$$

In this way, the initial values for k and ε may be calculated as:

$$k = 1.5 \cdot (V_{avg} I)^2 \tag{12}$$

$$\varepsilon = C_\mu^{3/2} \frac{k^{3/2}}{l} \tag{13}$$

where C_μ is an empirical constant specified in the turbulence model (approximately 0.09).

Outlet conditions:

Pressure, p (for subsonic conditions).

4.6. Numerical method

The *Fluent* code solves the system of partial differential equations in the form:

$$\frac{\mathrm{d}}{\mathrm{d}t} g + \frac{1}{V} \int_D \Phi(g) \cdot \underline{n} \, \mathrm{d}A = \dot{g}^+ \tag{14}$$

with

$$g = \frac{1}{V} \int_V G \, \mathrm{d}V, \qquad \Phi = \rho \underline{V} g + \underline{J}_G$$

where G is the generic unknown, g its density per unit volume, Φ the flux of g (convective + diffusive), $\underline{n}$ the unit vector normal to the surface D which encloses the control volume V, $\dot{g}^+$ the production of g per unit volume.

Equation (7) is discretized in space by substituting the sum with the surface integral:

$$\int_D \Phi(g) \cdot \underline{n} \, \mathrm{d}A = \sum_i \tilde{\Phi} \cdot \underline{n} A_i \tag{15}$$

The flux $\tilde{\Phi}$ is evaluated on the face A_i. The convective contribution is evaluated according to the *flux difference splitting* technique proposed by Roe [9]. The spatial accuracy is always of second order.

The integration is performed explicit in time by a *multigrid Runge–Kutta* scheme.

During the computation process, it is possible to refine the mesh where a more accurate solution is desired ("solution-adaptive grid").

5. NUMERICAL CODE VALIDATION. COLD TESTS

We performed some experimental and numerical tests at low values of enthalpy ($H_0 = 0.3$ MJ·kg^{-1}) in order to validate the numerical model. The arc heater was off, and the flow at the nozzle inlet was at ambient temperature.

Figure 3 shows the comparison between the measured experimental and computed numerical pressures along the diffuser wall, for a mass flow rate of 3 g·s^{-1} and for four different exit pressures. *Figure 4* shows the pressure in the test chamber as a function of the pressure at the diffuser exit. *Figure 5* shows the comparisons between numerical and experimental results at different mass flow rates (at the maximum capability of the vacuum system).

The numerical and experimental results are in good agreement at these conditions.

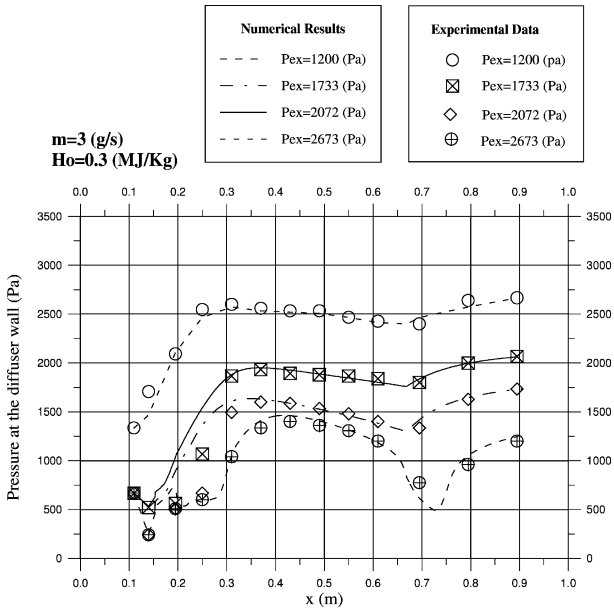

Figure 3. Cold tests: Pressures along the diffuser wall.

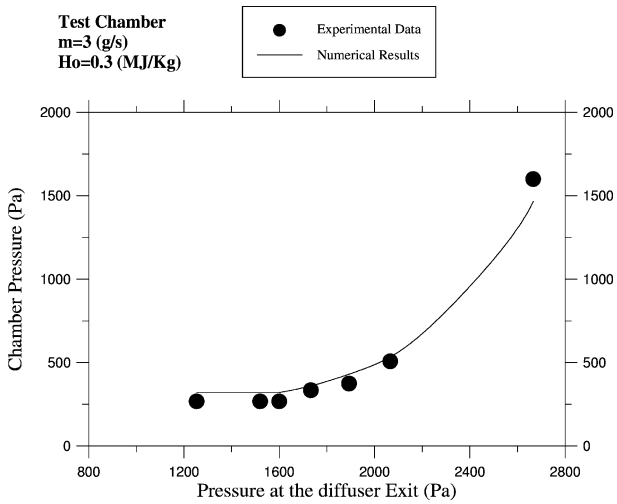

Figure 4. Cold tests: Pressure in the test chamber as a function of the exit pressure.

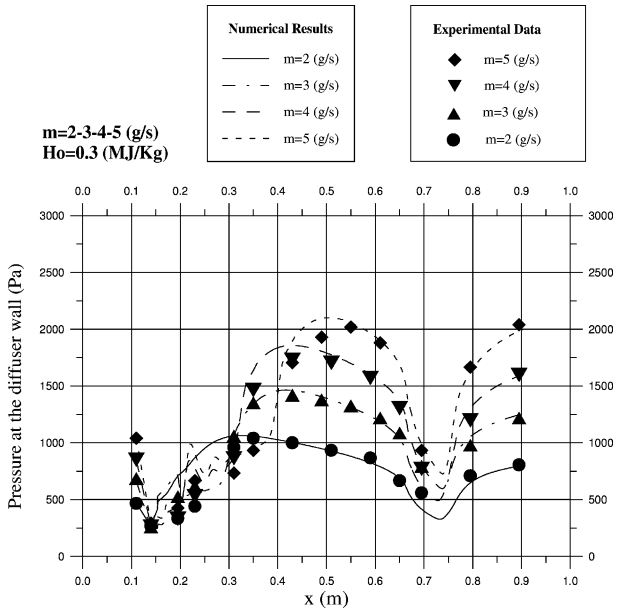

Figure 5. Cold tests: Pressures along the diffuser wall at different mass flow rates.

6. HIGH ENTHALPY RUNS

High enthalpy runs have been performed that basically consist in the measurements of a number of pressures along the diffuser.

Due to the lack of experimental data on the Nitrogen mass fraction (dissociation of N_2) at the nozzle inlet, chemical equilibrium conditions at the plasma torch

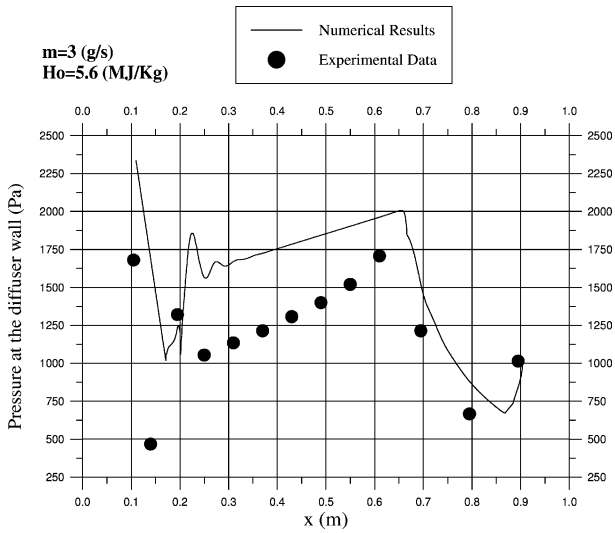

Figure 6. High Enthalpy runs, chemical equilibrium at the nozzle inlet: Numerical and Experimental pressures at the diffuser wall.

exit were initially assumed. The numerical results based upon this assumption were in disagreement with the experimental data. *Figure 6* shows the measured and computed pressures along the diffuser wall for a total enthalpy of 5.6 $MJ \cdot kg^{-1}$ and a mass flow rate of 3 $g \cdot s^{-1}$.

Figure 6 shows that the measured pressures along the diffuser wall were systematically higher than the computed pressures. These discrepancies were justified neither by the numerical approximations nor by the inaccuracy of the measurements.

We believe that one, or more, of the following points can give the reason for this disagreement:

(1) chemical equilibrium conditions at the nozzle inlet;

(2) uniform temperature and N concentration profiles at the nozzle inlet;

(3) vibrational equilibrium.

Our first thought was that point 3 was not of significant importance for the present test case. Indeed, to verify the influence of the hypothesis of vibrational equilibrium a number of numerical runs were performed, assuming a frozen vibrational degree of freedom. In fact, if we look at the expression of the specific total enthalpy:

$$H_0 = \int_{T_{\text{ref}}}^{T} c_{\text{p}}\,\mathrm{d}T + \frac{V^2}{2} + h_{\text{ch}} \qquad (16)$$

and if we remember that the specific heat is the sum of a translational, constant contribution, c_{pt}, and a vibrational contribution, c_{pv}, variable with the (vibrational) temper-

ature, we may write:

$$H_0 = c_{\mathrm{pT}} \cdot (T - T_{\mathrm{ref}}) + \int_{T_{\mathrm{ref}}}^{T} c_{\mathrm{pv}}\,\mathrm{d}T + \frac{V^2}{2} + h_{\mathrm{ch}} \quad (17)$$

where we assume that, at the nozzle inlet, the vibrational temperature is equal to the translational temperature, T. If we assume that the vibrational degree of freedom is frozen, the vibrational temperature remains equal to T throughout the flow field; the same holds true for the contribution $\int_{T_{\mathrm{ref}}}^{T} c_{\mathrm{pv}}\,\mathrm{d}T$, which can be calculated once at the beginning of the computations and subtracted from the effective value of the total enthalpy at the nozzle inlet, obtaining an *equivalent* total enthalpy. The calculations with the frozen vibrational process have been carried out assuming an equivalent total enthalpy at the nozzle inlet and considering only the translational part of the specific heats of the mixture components.

The results obtained show that the influence of the vibrational state of the gas molecules, even if moving in the right direction, was not so large to justify the discrepancy observed. Furthermore, the characteristic times of the recombination process are inversely proportional to the square of p while the characteristic times of the vibrational d.o.f. are inversely proportional to the first power of p, so that at the low pressures of the subject case (typically of the order of a hundred Pascal) the recombination process tends to be closer to frozen conditions when compared to the vibrational process.

In order to comprehend the influence of the hypotheses (1) and (2), we must consider which thermodynamic properties characterise the fluid downstream of the arc heater. In fact, the very high temperatures in the centre of the electric arc produce, in equilibrium, very high concentrations of dissociated Nitrogen. Typical (even if only qualitative) temperature and dissociated species distributions in an arc heater are depicted in *figure 7*.

If the temperature distribution in the arc region were uniform, as in our first hypothesis (*figure 7(a)*, equilibrium value), the corresponding equilibrium concentration of Atomic Nitrogen in the mixture would be much smaller than the average concentration for the non uniform flow, indicated in *figure 7(b)*. So we can state that the non-uniformity of the gas properties in the arc heater region is equivalent to a chemical non-equilibrium.

Therefore the flow that enters the still chamber that is located before the conical part of the nozzle is in local thermodynamic equilibrium, but is characterised

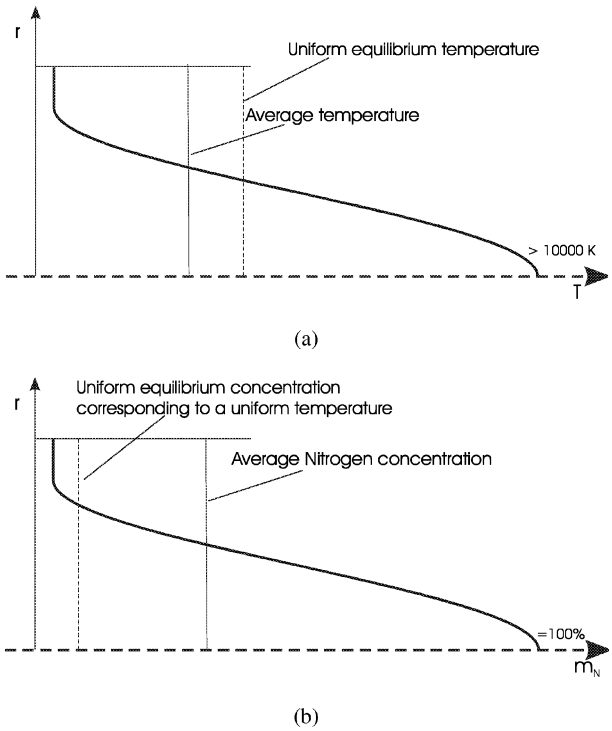

Figure 7. Qualitative distribution of: (a) temperature, and (b) atomic Nitrogen concentration downstream of an arc heater.

by strongly non uniform distributions of properties such as temperature and species concentrations. At this point there are two possibilities:

(1) the flow is mixed in equilibrium,
(2) a frozen mixing occurs.

In the first case we would return to the initial situation corresponding to equilibrium conditions at the nozzle inlet. In the second case, the "fictitious" chemical non-equilibrium due to the non-uniformity would partly remain in the flow and the following development of the flow field in the diffuser could be much different than in the previous case. Computations of the nozzle flow field, performed with the finite rate chemistry hypothesis, show that the situation described by point 2 is established. Therefore we hope that with these new initial conditions the agreement between numerical and experimental data is better.

In order to compute realistic chemical conditions at the nozzle inlet, a study on the behaviour of the plasma torch, supported by a bibliographic investigation, was performed. These new initial conditions were then used to start the new computations of the nozzle and diffuser flowfield of HEBDAF.

6.1. Numerical simulation of the arc heater

Due to the electrical current flow (discharge) inside the fluid, and to the electromagnetic forces, we can assume the configuration for the electric arc [10–13] in *figure 8(a)*.

A correct simulation of the heat addiction in the electric arc should be done through the solution of the Navier Stokes' equations coupled with the Maxwell's equations. The Fluent code is not able to compute the thermo-fluid-dynamic field at these conditions. However, through some simplifying hypotheses, it was possible to perform a relatively simple numerical simulation of the flow field in the plasma torch.

Electro-magnetic phenomena were neglected, and the flow was assumed axisymmetric.

The plasma torch has been modelled as a constant section duct; the arc shape (where electrical energy is supplied to the gas) is illustrated in *figure 8(b)*. The power supplied to the gas is taken into account as a source term (per unit volume) in the energy conservation equation, dividing the arc electrical power by the volume of the arc region.

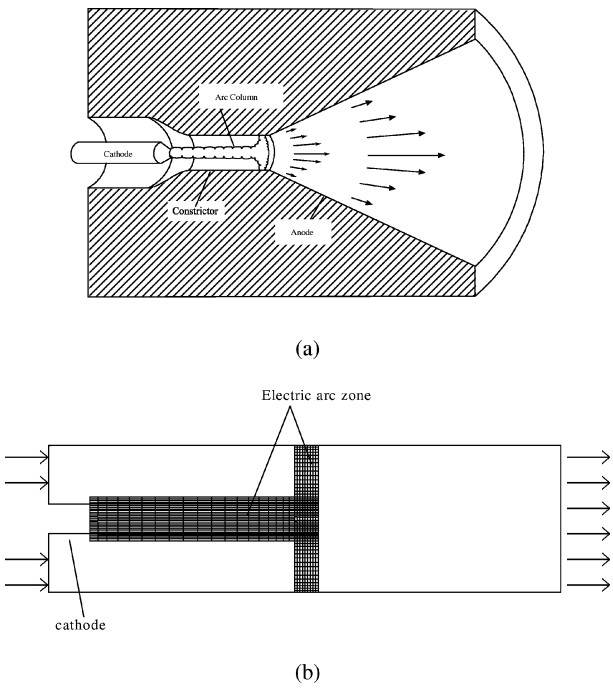

Figure 8. (a) Schematic arrangement of the electrical discharge inside a plasma torch; (b) Torch model with the electric arc discharge zone.

The N^+ ions were assumed to have the same transport properties of the atomic Nitrogen. The presence of free electrons is not taken into account.

The ionisation reaction for atomic Nitrogen:

$$N \leftarrow\rightarrow N^+ + e \tag{18}$$

was considered together with the N_2 dissociation (already considered in the previous model). The reaction rate constants are taken from the Dunn–Kang model.

The numerical simulations have been performed assuming that Nitrogen is initially at ambient temperature. The code computes, for given mass flow rate and arc power, the thermo-chemical properties of the gas mixture at the torch exit.

Typical profiles of specific total enthalpy at the torch exit are shown in *figure 9*.

Figure 10 shows the species mass fractions distributions at the torch exit. It turns out that the flow at the nozzle inlet is locally in chemical equilibrium but in strong non-uniform conditions for the distributions of temperature and chemical species, as anticipated in the previous section.

Since the Fluent code is able to perform numerical simulations assigning non uniform inlet conditions, we have performed numerical computations starting from the computed field at the plasma torch exit. The differences for the pressures on the diffuser wall, for the two cases of "uniform" and "non uniform" inlet conditions, are not appreciable (i.e., less than 1%). On the other hand the other fields show appreciable differences. For instance, the temperature distribution is much different before the nozzle throat in the two cases, while it is nearly identical

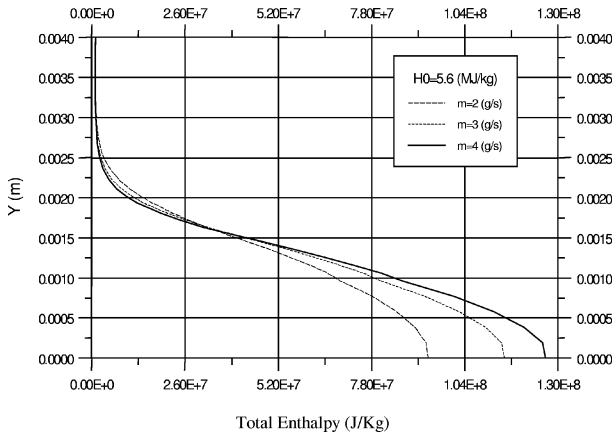

Figure 9. Total enthalpy profiles at the torch exit as functions of mass flow rate.

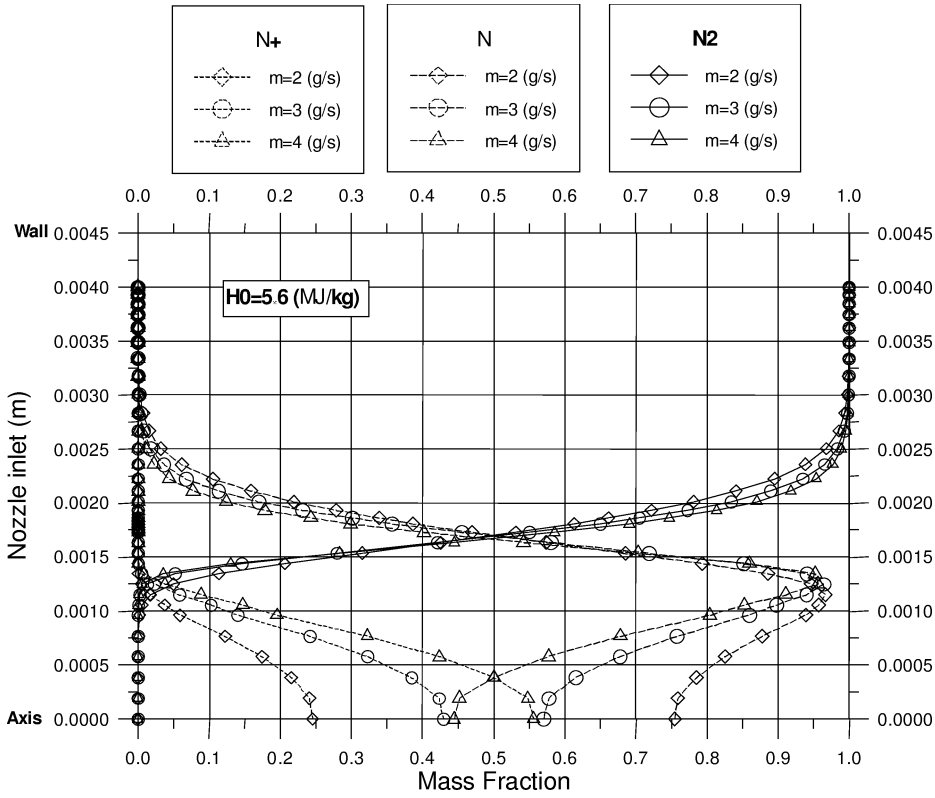

Figure 10. Profiles of the species mass fractions at the torch exit for different mass flow rates.

at the nozzle exit and in the diffuser, due to the turbulent mixing occurring from the nozzle divergent.

7. DESCRIPTION OF THE RESULTS

Several numerical runs have been performed to reproduce the experimental tests, characterised by gradually increasing values of the pressure at the diffuser exit.

The behaviour of the flow has been described in [14]: the shock waves are initially located in the divergent part of the diffuser and move backward to the test chamber at larger exit pressures.

Figures 11–14 show the comparison between the numerical and experimental pressures at the diffuser wall for different exit pressures. The estimated error on each experimental measure is no more than ± 60 Pa.

This comparison is now remarkably better than before (*figure 6*).

When the exit pressure is low enough a shock wave is located in the diverging part of the diffuser. Starting from

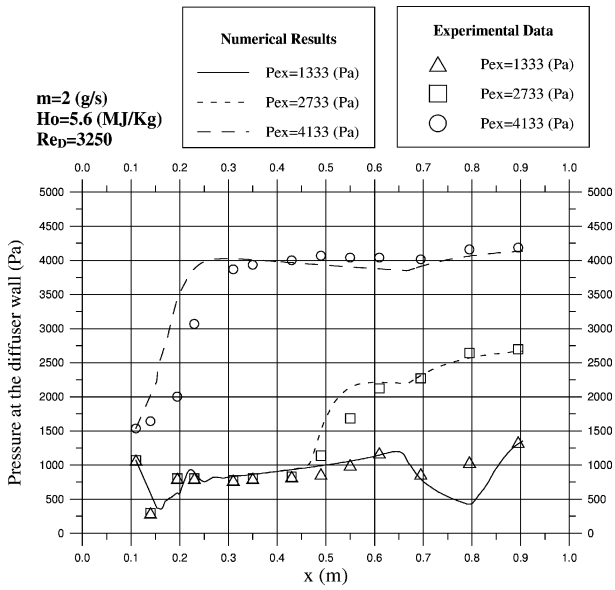

Figure 11. Pressure distribution along the diffuser wall for different exit pressures ($m = 2$ g·s^{-1}; $H_0 = 5.6$ MJ·kg^{-1}).

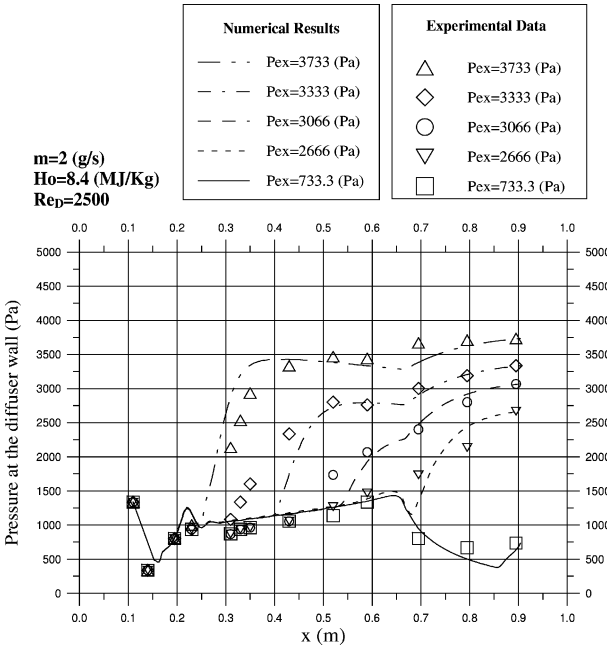

Figure 12. Pressure distribution along the diffuser wall for different exit pressures ($m = 2$ g·s^{-1}; $H_0 = 8.4$ MJ·kg^{-1}).

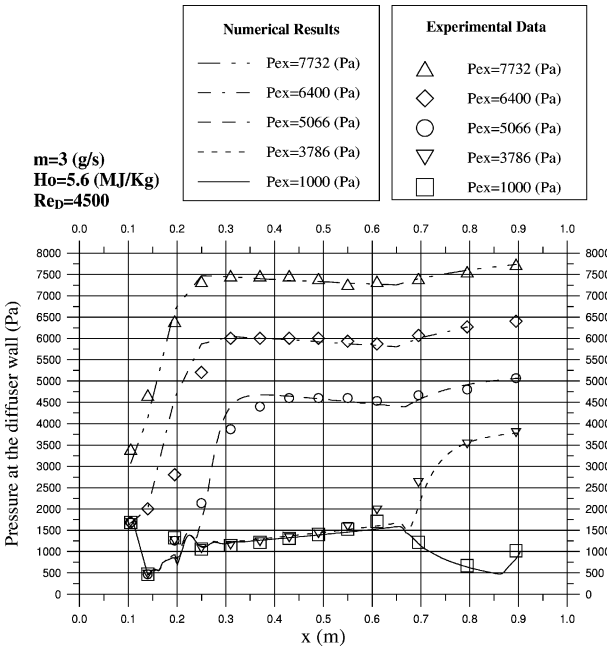

Figure 13. Pressure distribution along the diffuser wall for different exit pressures ($m = 3$ g·s^{-1}; $H_0 = 5.6$ MJ·kg^{-1}).

the nozzle exit, a sudden flow expansion occurs in the test chamber, before the diffuser inlet, reaching a Mach

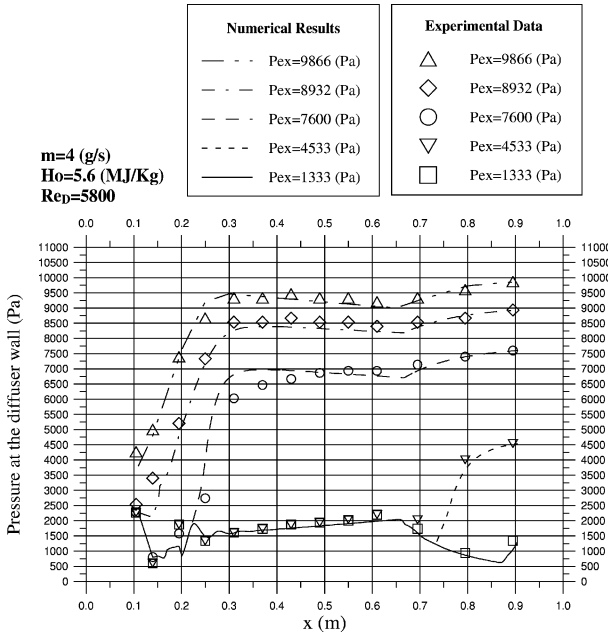

Figure 14. Pressure distribution along the diffuser wall for different exit pressures ($m = 4$ g·s^{-1}; $H_0 = 5.6$ MJ·kg^{-1}).

number of about 5 at the diffuser inlet. The flow field is characterised by a number of shock and expansion waves, which decelerate the supersonic flow. The expansion in the diverging part terminates with the final shock wave necessary to reach the exit pressure.

The turbulence model is essential to reproduce the experimental results by numerical computations (laminar computations do not correlate the experimental results). The good agreement of the turbulent simulations is also justified by the values of the Reynolds number (see *figures 11–14*), which are all greater than or equal to the critical Reynolds number, $Re_{cr} \cong 2500$.

8. CONCLUSIONS

The present study focuses on the analysis of low-Reynolds supersonic diffusers. The study has been performed on both experimental and numerical grounds. The experimental tests have been carried out at the DISIS plasma wind tunnel facility, HEBDAF. The numerical work has mainly dealt with the definition of a physical-mathematical model able to correctly describe the flow features; in particular, an approximate fluid-dynamic model of the arc-heater has been realised.

The experimental data and the numerical results based on the above assumptions are in good agreement.

The results show the following:

• The wind tunnel operations are strongly influenced by the thermo-chemical conditions of the flow. Indeed, the numerical-experimental comparison has highlighted the non-uniform and chemical non-equilibrium conditions of the flow at the plasma torch exit section (nozzle inlet).

REFERENCES

[1] Hanus G.J., Mikkelson K.L., Olstad S.J., Caristia S., Supersonic wind tunnel diffuser performances with high model blockage at moderate to low Reynolds number, AIAA 91-2274, AIAA/SAE/ASME/ASEE/ 27th Joint Propulsion Conference, Sacramento, CA, 24–26 June 1991.

[2] Schettino A., Serpico M., Analisi del funzionamento del diffusore di Scirocco, CIRA Internal Report, 1997.

[3] Monti R., Ferrigno F., De Rosa F., Esposito A., Studio di un diffusore supersonico ai bassi numeri di Reynolds sull'impianto HEBDAF, DISIS Internal Report 97–02, 1997.

[4] Fluent User's Guide, Fluent Inc., 1998.

[5] Blottner F.G., Jonson M., Hellis M., Chemically reacting viscous flow program for multi component gas mixture, Technical Report SC-RR-70-754, SANDIA, 1971.

[6] Hoffman K.A., Chiang S.T.L., Siddiqui M.S., Fundamental equations of fluid mechanics, in: Publication of Engineering System™, Wichita Kansas, USA, 1997, pp. 272–317.

[7] Launder B.E., Spalding D.B., Lectures in Mathematical Models of Turbulence, Academic Press, New York, 1971.

[8] Favre A., Statistical equations of turbulent cases, in: Problems of Hydrodynamic and Continuum Mechanics, SIAM, Philadelphia, 1969, pp. 231–266.

[9] Jameson A., Schmidt W., Turkel E., Numerical solution of the Euler equations by finite volume methods using Runge–Kutta time-stepping schemes, Technical Report AIAA-81-1259, AIAA 14th Fluid and Plasma Dynamics Conference, Palo Alto, CA, June 1981.

[10] Miller S.A., Martinez-Sanchez M., Two fluid non-equilibrium simulation of hydrogen arcjet thrusters, J. Propulsion Power 12 (1) (1996) 112–119.

[11] Hargus W.A. Jr., Cappelli M.A., Pressure measurements in the plume of a low power arcjet nozzle, High Temperature Gasdynamics Laboratory, Mechanical Engineering Department, Stanford University, 1996.

[12] Hargus W.A. Jr., Cappelli M.A., Mass flux measurements in the plume of a low power arcjet nozzle, High Temperature Gasdynamics Laboratory, Mechanical Engineering Department, Stanford University, 1996.

[13] Black N.A., Fradkin D.B., Macroscopic analysis of magnetoplasmadynamic arc jets, L.A. 3736 UC-34, PHYSICS TID-4500, 1995.

[14] Monti R., Esposito A., Savino R., Ferrigno F., Schettino A., Serpico M., Experimental and numerical analysis of low-Reynolds numbers hypersonic diffusers, AIDAA, Napoli, 1997.